Chapter 5

Commissioning the Instrument

Once the assembling of the instrument in the laboratory was completed, a series of commissioning tests were carried out to verify that the instrument stands up to the performance targets specified at the onset of the project. These tests provided quantitative estimates of various parameters which characterize the instrument. The commissioning tests were carried out in two phases – first a set of tests on the laboratory optical bench which was followed by observations with the instrument at a telescope. This chapter primarily discusses these tests and their results. The first section discusses the laboratory phase of commissioning while the one following it presents the results of observations with the telescope.

5.1 Phase I - The Laboratory Tests

Two sets of tests were conducted on the laboratory optical bench. The first was to determine parameters of the CCD camera like its gain, readnoise, linearity, intra-pixel sensitivity variation etc. and the second to look for scattering in the optics and to estimate self-polarization and depolarization in the instrument.

5.1.1 CCD camera characteristics

Gain : The gain (G) of the CCD camera is defined as the number of photoelectrons which correspond to one ADU count. A standard way of measuring this parameter is the variance method which is based on the poissonian nature of the distribution of photoelectrons. Essentially, the variance (σ_N^2) associated with the detection of N electrons is given by

$$\sigma_N^2 = N \; . \tag{5.1}$$

Multiplying both sides with $A^2 = (\frac{1}{G})^2$, we obtain

$$A^2\sigma_N^2 = A^2 N \; . \tag{5.2}$$

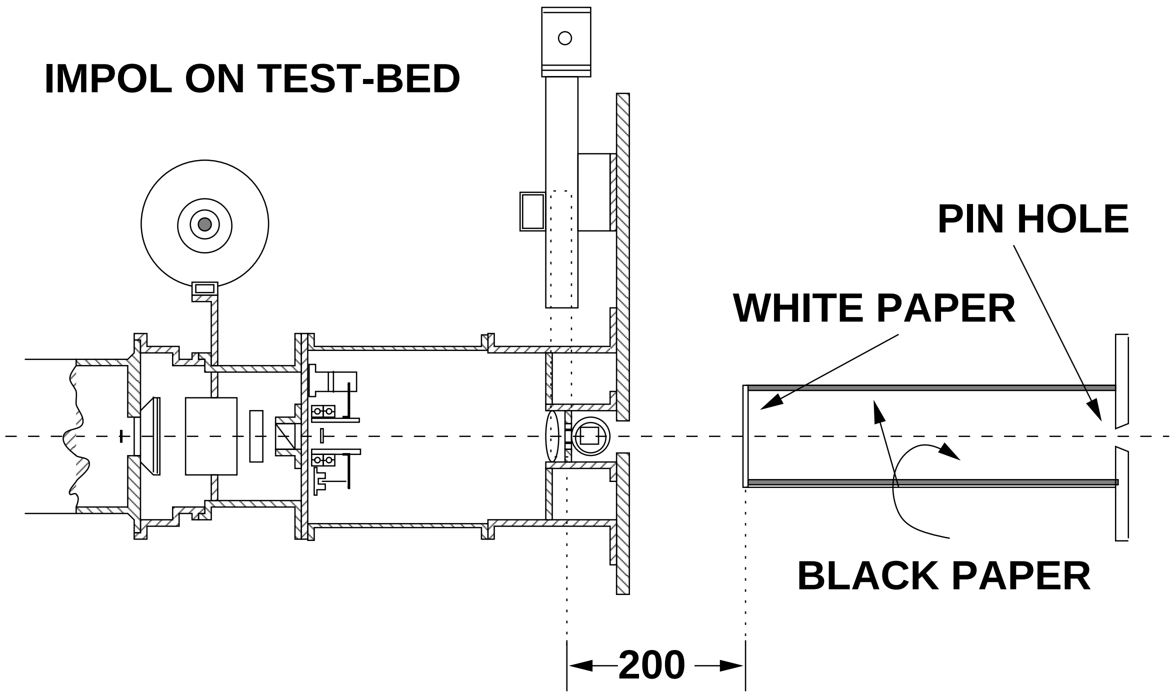

Figure 5.1: Setup for determining the gain and readnoise of the CCD camera

The number (N_{ADU}) of ADUs which correspond to N photoelectrons is, by definition, given by

$$N_{\mathrm{ADU}} = AN \qquad \text{and hence} \qquad \sigma^2_{N_{\mathrm{ADU}}} = A^2 \sigma^2_N \; . \tag{5.3}$$

Substituting the relations in Eq. 5.3 into Eq. 5.2, we get

$$\sigma^2_{N_{\mathrm{ADU}}} = A N_{\mathrm{ADU}} \qquad \text{or equivalently,} \qquad G = \frac{N_{\mathrm{ADU}}}{\sigma^2_{N_{\mathrm{ADU}}}} \; . \tag{5.4}$$

Therefore, the gain of the CCD camera may be determined by taking a uniformly illuminated image and finding the ratio of mean ADU counts to the variance in the counts. In order to eliminate effects caused by pixel to pixel sensitivity variations, the variance may be determined from the counts at the same pixel position in a set of identical exposures.

The setup devised for determining the gain is shown in Fig. 5.1. The instrument is fixed on its test mounting plate on the laboratory optical bench. A uniformly illuminated extended source is simulated in the following way. The opening at one end of a long pipe, about 90 mm in diameter, is covered with white paper. The inside of the pipe is blackened and a pinhole source is placed at the centre of its second opening. The pipe is placed so that the end covered with white paper is directly in front of the grid and some 200 mm in the front. This ensures that the plane of the paper is sufficiently far away from the grid surface, which is reimaged on to the CCD, so that the graininess of the paper as well as any small scale changes in its illumination are smoothed out.

A succession of image frames as well as dark frames of same exposure duration are taken with this setup. The illumination of the paper and the exposure duration are adjusted so that the pixels are about 80% filled. The pixel counts in each frame is multiplied by a factor, so that the total pixel count is the same for all the frames. An average image frame is created in which the ADU count at each pixel position is equal to the average of the counts at the same position in all the image frames. Similarly an average dark frame also is created which is subtracted from the average image frame. Now a 25×25 pixel box is chosen in the average frame and the mean pixel value there is noted. This is our estimate of N_{ADU}. The averaging process described above is to minimize the influence of cosmic rays, hot spots etc. in the measurement. From the same pixel box position in each of the image frames, the variance of the pixel counts is determined for each pixel. The average of these variances is our estimate of $\sigma^2_{N_{\mathrm{ADU}}}$. Substituting these values in the second expression in Eq. 5.4, will give the value of G. The CCD used in IMPOL has a gain of about 5 electrons per ADU.

Readnoise : The readnoise measures the CCD camera's noise contribution while converting the electrons which are collected in a pixel to ADU counts. If the exposures taken in the above experiment are of sufficiently small duration so that the counts in the dark frames are not much above the zero level, the readnoise can be easily determined. For this a difference frame is created in which the ADU count at each position is equal to the difference between the counts at the same position in two of the dark frames. Again, a 25×25 pixel box is chosen and the standard deviation of the counts in the box is $\sqrt{2}$ times the readnoise of the CCD camera. For this camera the readnoise is about 1.6 ADU counts or about 8 electrons.

Linearity : A linear device generates an output which is directly proportional to the input. But in this particular application, we are more concerned about the ratios of intensities at two different locations on the CCD, than on their absolute values. The requirement for polarimetry is satisfied, as long as the ratios stay constant independent of the exposure time, for a given illumination. The experimental setup used for this is almost identical to that used to produce the flat fields in the case of measuring gain, except that here a sheet polarizer has been introduced so that it covers half of the grid (see Fig. 5.2).

Image and dark frame pairs are taken with several different exposure durations and each dark frame is subtracted from its corresponding image frame. A pair of points is chosen on one of the dark-subtracted frames so that one of them is in the region covered by the polarizer and the other outside. Since the shutter movement may cause variations in the effective exposure durations, it is advisable to choose these points as close as possible. The ratio of the mean ADU counts within a 25×25 box, centred on these points are noted. This is repeated for each of the dark-subtracted frame pairs, but at exactly the same pixel positions as in the first frame. It was found that the dispersion in this ratios is less than 0.1%. This process is repeated for other sets of point pairs on the frames.

Intra-pixel sensitivity variation : It is known that the sensitivity of a pixel depends very much on where on it, the light falls. This experiment was carried out to quantify

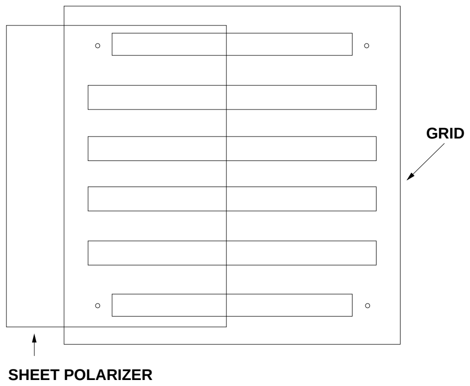

Figure 5.2: A sheet polarizer is placed covering half of the grid, for testing the linearity of the CCD camera.

the effect of this for IMPOL's CCD camera and the setup used is shown in Fig. 5.3. The pinhole is mounted on an translation stage with vernier readings, so that it can be moved in a plane orthogonal to the instrument axis, with 10 μm positional accuracy. A camera lens is used to focus the pinhole on the grid surface which is reimaged within the instrument on to the CCD. The FWHM of the image on the CCD is kept to be about 3 pixels, which is similar to the FWHM of the point-spread function of the stellar images. Two exposures are taken and the ratios of the counts in the ordinary and the extraordinary images in them are noted and the average of these two ratios is calculated. It is ensured that sufficient number of photoelectrons are collected so as to keep the photon noise in the determination of these counts, as low as 0.1%. Now the pinhole is moved by about 80 μm so that the image on the CCD moves by about one tenth of a pixel and the mean of the ratios determined as above. This process is repeated for about twenty positions of the pinhole. It was found that the peak to peak range of the ratios was about 0.1%. A necessary implication of this finding is that in order to achieve good polarimetric accuracy, the FWHM of the point-spread function should be about 3 pixels or more.

5.1.2 Characterization of the optics

The purpose of these tests were to ensure that the instrument optics performs sufficiently well to achieve the demanded accuracy in polarimetric measurements. If stray light, scattering within the instrument reaches the CCD, it will affect the measurement of intensities and thereby the polarimetric accuracy. The first test was designed to look for instrumental scattering, particularly from the edges of components mounts etc. The instrument optics can introduce polarization into initially unpolarized light, due to a variety of causes and this sets the limit to the polarization measurement accuracy that can be achieved with the instrument. Another source of error in polarization measurements is the conversion of linearly polarized light into circular or unpolarized light. Mainly, three tests were carried out in the laboratory, to determine the extent to which these effects take place in this instrument.

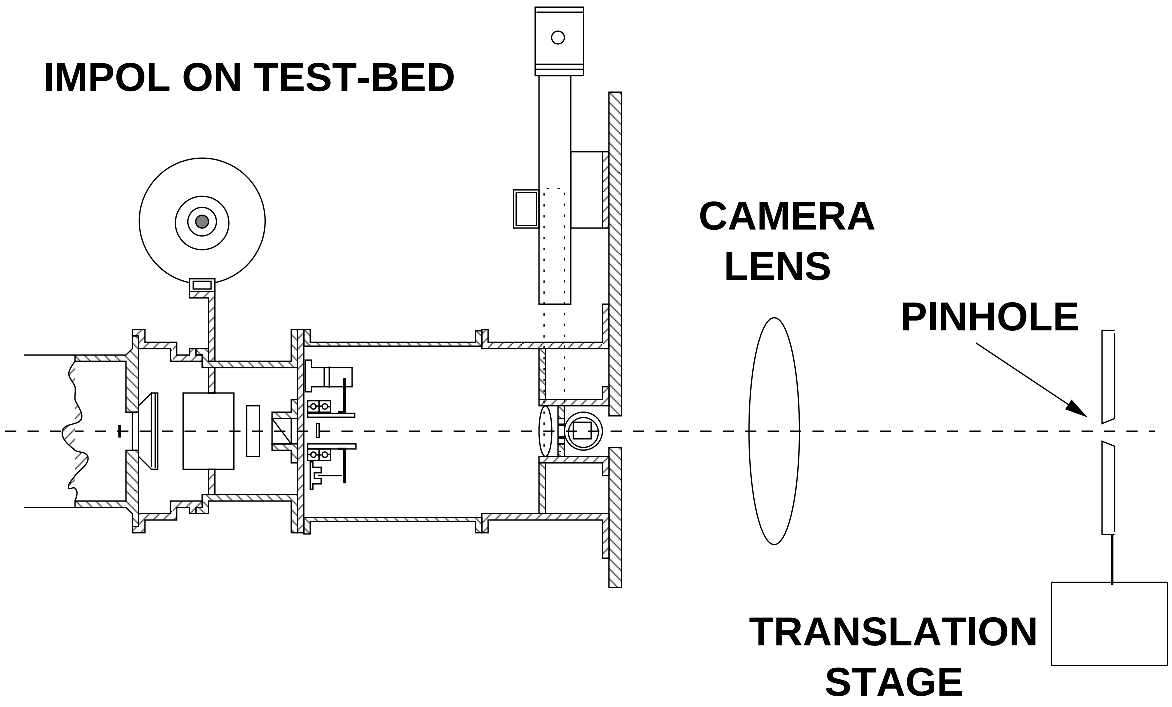

Figure 5.3: Setup used to determine the intra-pixel sensitivity variation of the IMPOL CCD camera

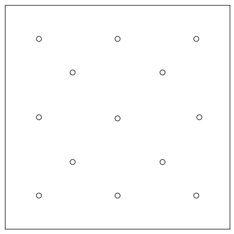

Figure 5.4: The pinhole mask placed at the position of the CCD surface while looking for scattering within the instrument.

Scattering of light within the instrument : Since the instrument optics is well-matched with the telescope beam, with the HWP acting as the aperture stop (see Sec. 2.2 and 2.3.4), there is little chance of scattered light, reflecting from the walls etc. reaching the CCD detector. Nevertheless it was verified that this is so. The CCD dewar was removed from the instrument assembly and a mask with 1 mm diameter pinholes as shown in Fig. 5.4 was placed at the position of the CCD surface. The instrument is illuminated through the grid at the front end with an ordinary filament lamp source. By viewing carefully through the pinholes, the parts which appear to scatter light are noted. The only part which appeared vulnerable enough to cause any trouble was the ground edges of the HWP which scattered light.

The HWP assembly was modified slightly, as shown in Fig. 5.5 to prevent light from scattering at the edges of the HWP. For this, a small black ring which just covers

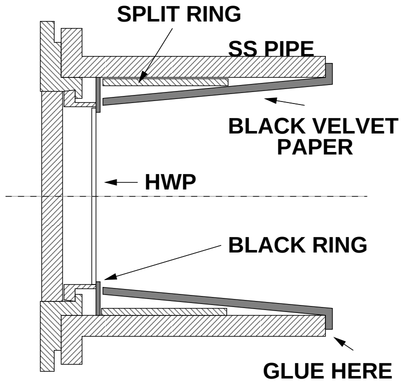

Figure 5.5: Section of the modified HWP mount which prevents scattering from the HWP edges.

the HWP edges is kept pressed against the HWP surface, by a split ring. A sheet of black velvet paper folded into a cone is fixed inside the SS pipe, (see Fig. 5.5) in which the HWP sits, so as to reduce light reflecting from the walls of the pipe.

Depolarization : The experimental setup used for checking depolarization within the instrument is shown in Fig. 5.6. A slightly defocussed image of a pinhole is formed on the grid surface using a lens so that the beam is f/13 and the FWHM of the images on the CCD is about 3 pixels. A polarizer (HN22) is inserted in the beam path and observations are made in the B, V and R wavelength bands. Care is taken to collect sufficient photons in the images to keep the photon noise below 0.01%. Polarization measurements gave 99.6% in the B and V bands and 94.6% in the R-band. Measurements with a wideband filter which transmits both V and R bands, gave 94.6% polarization. The HN22 polarizer performance curves show that it is optimized for operation in the V-band. This probably explains why the the apparent depolarization is over 5% in the R and wide bands.

Instrumental polarization : Instrumental polarization refers to the measured value of polarization when the input light beam is unpolarized and it indicates the level of sensitivity that can be attained with the instrument. To determine the instrumental polarization, again the f/13 beam setup is used, as in the previous case but a Lyot depolarizer is inserted in the beam path this time. Polarization measurements gave $p \sim 0.03\%$ in the B-band and 0.06% in the wideband filter, which is mentioned above. The position angle of the polarization vector for the wideband was about 5°. Now the Lyot depolarizer is turned by 90°and another measurement is made. This time the degree of linear polarization, for the wideband was found to be 0.08% and oriented at 96°. This indicates that most of the enhancement in the instrumental polarization in the wideband is due to the performance degradation of the depolarizer. In order to check if there is any instrumental polarization due to scattering of light, the beam size was reduced to f/20. This measurement in the wideband, again gave about 0.08% polarization.

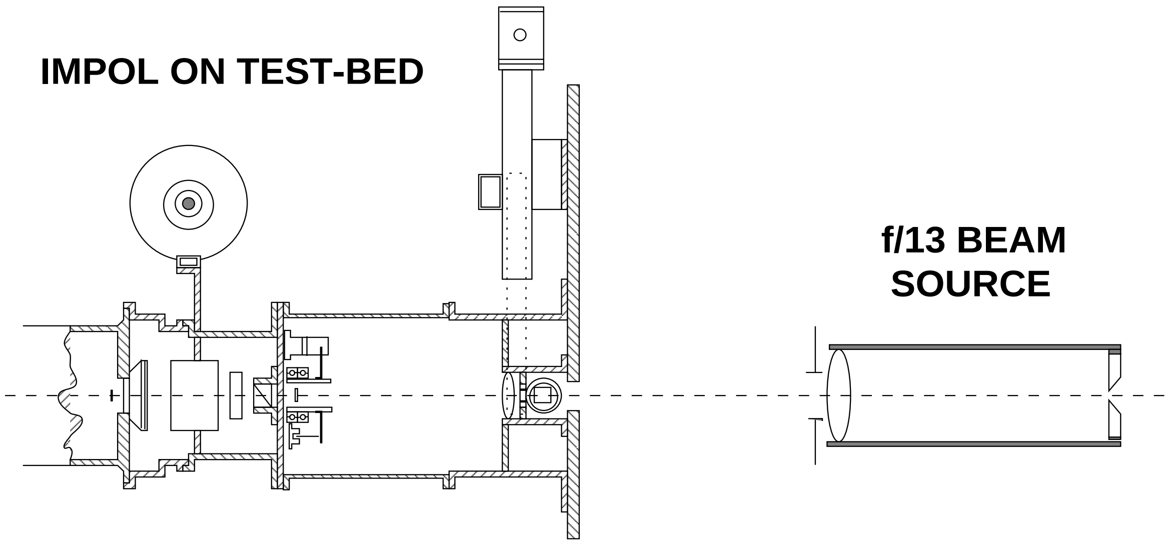

Figure 5.6: Setup used for checking depolarization.

5.2 Phase II - Tests on the telescope

The second stage of tests were conducted when the instrument saw the first light in February 1996, at the 1.2 m diameter GIRT at Mt. Abu. Several standard polarized and unpolarized stars were observed at this time. Since the available standard stars are all very bright, having visual magnitudes in the range of 4 to 7, instrument was slightly defocussed to avoid saturation of pixels in reasonable exposure times.

Table 5.1 contains the results of the observations in V-band. Column 1 of the table gives the identification number of the star. Columns 2-5 contain the measured values and 1σ errors of the fractional polarization p and the position angle θ. Column 6 gives an estimate of the error σ_{phot}, based on photon statistics alone, derived as given in Eq. 3.14. Cols. 7 and 8 list the published values of p and θ (Serkowski 1975). The first two stars in the table are polarized standards while the last two are unpolarized ones. The four measurements of star HD39587 are made at different corners of the CCD frame in order to verify the uniformity of response. Comparing the measured and published results for the polarized stars we see that there is no indication of depolarization. Neither is there any rotation of the position angle beyond a couple of degrees. From Col. 3 and Col. 6 for the unpolarized stars, we see that the error in the measured polarization is comparable with that expected on the basis of photon statistics alone, and hence it can be concluded that the instrumental polarization is less than 0.03%.

In Fig. 5.7, the values of $q = R(0°)$ are plotted against $u = R(22.5°)$ for all the unpolarized standards observed in the V-band. The extremely low correlation coefficient between q and u, is indicative of the low instrumental polarization, which otherwise would show up as clustering in the distribution of points in the graph. The average values of q and u, give a value of polarization $p = 0.03\%$ which is consistent with

Table 5.1: Observations of standard stars

Star	p	σ_p	θ	σ_θ	$\sigma_{\rm phot}$	p_0	θ_0
(1)	(2)	(3)	(4)	(5)	(6)	(7)	(8)
HD	%	%	°	°	%	%	°
43384	3.05	0.04	172	0.3	0.03	3.0	170
154445	3.65	0.03	90.5	0.2	0.02	3.7	90
102870	0.03	0.01	64.4	7.8	0.02	0.017	162
39587	0.03	0.03	140	27.5	0.02	0.013	20
	0.05	0.02	159	12.7	0.02		
	0.09	0.02	34	6.7	0.02		
	0.05	0.02	167	11.3	0.02		

the values obtained in the laboratory tests. These observations show that for accuracies $\gtrsim$0.05% in the measurement of polarization p, the performance is still limited by photon noise and the instrumental polarization floor has not yet reached.

In Fig. 5.8 the solid and dashed curves show how the error in the measurement of fractional polarization, based on photon statistics alone, changes as a function of source brightness, for two types of sources, namely point sources (eg. stars) and extended sources (eg. reflection nebulae) respectively. Polarimetry of standard stars background to the Bok globule B 133, was carried out during the commissioning observations. The points marked in the figure show the 1σ errors in the measurement of p, against the visual magnitude of the stars. The very good matching of the photon-noise estimate curve with these points, indicate that the polarimetric accuracy, here, is limited by photon noise.

The information which is required to incorporate the acquisition and guidance (A&G) system was also collected during this observation run. This included the coefficients of the equations of transformation from the A&G CCD pixel coordinates to the main CCD pixel coordinates, the correspondence between the relays and the telescope axes, the gain of the system in terms of telescope motion per unit time of relay activation, linearity of the gain as a function of relay activation time etc. The A&G system was successfully installed during a second observation run with the same telescope in late May, 1996. Observations made at this time showed that the A&G system is capable of acquiring and tracking on stars as faint as V=15, with accuracies as good as a fraction of an arcsecond.

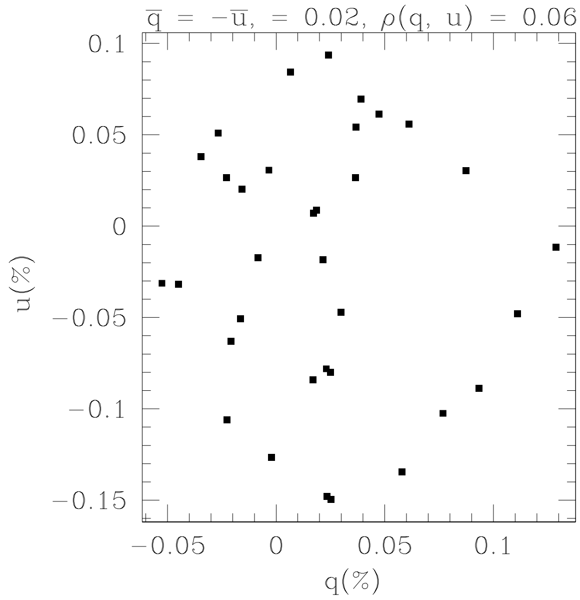

Figure 5.7: Normalized Stoke's parameter q is plotted against u for a number of unpolarized standard stars. The correlation coefficient of the points is about 0.06 and the average values of q and u give a value of $p = 0.03\%$.

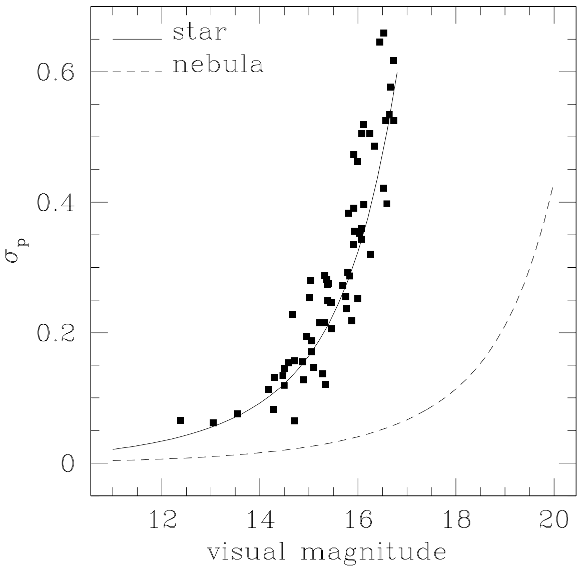

Figure 5.8: The errors due to photon noise alone, for wideband measurements of fractional polarization p are shown as a function of the brightness of the source. The solid curve refers to the case of stars while the dashed curve is for an extended object, for which the x-axis represents the surface brightness of the source in magnitudes per sq. arcsecs. The background is assumed to be 20^{th} magnitude per sq. arcsec and a software aperture of 30 sq. arcsec has been used during data reduction. The points marked represent the errors in actual polarimetric measurements made with instrument on a field at the periphery of the dark cloud B133.